frontiers | Frontiers in Materials

ORIGINAL RESEARCH
published: 16 June 2022
doi: 10.3389/fmats.2022.909006

Three-Dimensional Impact Localization on Concrete Structures Using Novel Enhanced Cross-Correlation Algorithm and Designed Concrete Implantable Module

Qingjun Chen[1,2], *Ziqian Yang*[1,2], *Xiuquan Li*[1,2], *Xiangtao Sun*[1,2] *and Qingzhao Kong*[1,2]*

[1]State Key Laboratory of Disaster Reduction in Civil Engineering, Tongji University, Shanghai, China, [2]Department of Disaster Mitigation for Structures, Tongji University, Shanghai, China

Concrete structures are often subjected to undesirable impact loads. Impact localization in near real time is greatly essential for providing early warnings and evaluating impact load effects. In this article, a novel enhanced cross-correlation (ECC) algorithm enabled by a designed concrete implantable module (CIM) is proposed for precise prediction of the impact location on concrete structures. The stability of the ECC algorithm under the noise condition was numerically studied. The numerical results demonstrate that the proposed ECC algorithm has high adaptability in the low signal-to-noise ratio (SNR) condition compared with the traditional algorithm, which provides the possibility for employing this approach in real projects. In the experimental study, a series of impact tests on a concrete beam specimen were conducted to verify the accuracy of the proposed method for impact localization. The results indicate that the maximum and minimum distance errors between the real and predicted impact positions are 54.1 and 12.5 mm, respectively. Both the numerical and experimental studies demonstrate the feasibility of the proposed method for the prediction of impact locations.

Keywords: concrete implantable module, spherical piezoceramic shell, enhanced cross-correlation algorithm, time difference of arrival, time of flight, structural health monitoring

OPEN ACCESS

Edited by:
Siqi Ding,
Harbin Institute of Technology, China

Reviewed by:
Venu Gopal Madhav Annamdas,
Continental Automotive Singapore, Singapore
Tianhong Yan,
China Jiliang University, China

***Correspondence:**
Qingzhao Kong
qkong@tongji.edu.cn

Specialty section:
This article was submitted to Smart Materials, a section of the journal Frontiers in Materials

Received: *31 March 2022*
Accepted: *10 May 2022*
Published: *16 June 2022*

Citation:
Chen Q, Yang Z, Li X, Sun X and Kong Q (2022) Three-Dimensional Impact Localization on Concrete Structures Using Novel Enhanced Cross-Correlation Algorithm and Designed Concrete Implantable Module. Front. Mater. 9:909006. doi: 10.3389/fmats.2022.909006

INTRODUCTION

Maintaining structural safety and providing early warning is a permanent mission for the development of structural health monitoring (SHM) in civil engineering (Ko and Ni, 2005; Rainieri et al., 2011; Kao and Loh, 2013; Feng et al., 2020; Fan et al., 2021a; Chen et al., 2021). The long-term and unceasing operation of a structure will face various challenges from the internal and external loads. Impact loads, due to their strong energy and instantaneous action, can suddenly attack the structures; most of them have no enough time to warn and resist (De Fenza et al., 2017; Fan et al., 2018; Tian et al., 2019). On 9 May 1980, the pier of Sunshine Skyway Bridge was collided by a freighter with a sudden squall and collapsed into the bay (Asencio-Rhine, 2020). On 11 May 2021, due to the Palestine–Israel conflict, a 13-storey residential tower in the Gaza strip was air stuck by a high-speed missile and collapsed soon (Kocherla et al., 2021). The impact loads induced structural

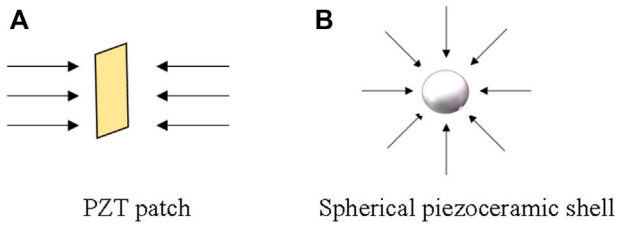

FIGURE 1 | Principle of receiving signals from different PZT elements. **(A)** PZT patch. **(B)** Spherical piezoceramic shell.

damages that seriously threaten human safe and economic development. Therefore, fast and accurate localization of the impact sources is greatly significant for the structures to warn early and defend in time.

Acoustic emission (AE) source localization, a nondestructive test (NDT) technique, plays a vital role in SHM (Perelli et al., 2012; Schechinger and Vogel, 2007; Tsangouri et al., 2016; Xu et al., 2016). The AE sources, deriving from structural internal sudden cracking or external accidental collision, can generate mechanical waves propagating in the structures. Meanwhile, by implementing some sensors on these structures, their dynamic responses can be recorded and used to quantitively analyze the acoustic source location. Based on this, the AE source localization technique has been widely applied in the fields of aerospace, mining engineering, navigation, and other various structure detection (De Simone et al., 2017; Dong et al., 2017; Zhang et al., 2017). In civil engineering, the investigations of this technique in metal structures such as aluminum and steel are far more simple than those in concrete members due to their complex material properties, such as anisotropy and nonlinearity (Ebrahimkhanlou and Salamone, 2017; Ebrahimkhanlou and Salamone, 2018; Sedlak et al., 2013; Wang et al., 2020). However, concrete, the most common building material, has many excellent characteristics in resistance of collision, corrosion, and fire disasters (Aitcin, 2003; Hao et al., 2016; Murthy et al., 2010). At the same time, the impact accidents happening on concrete structures are reported very frequently every year. Therefore, studying the impact source localization in concrete structures is necessary and significant. Barbara *et al.* studied the accuracy of the AE localization in a concrete beam under a loading test (Schechinger and Vogel, 2007). Zhu et al. (2017) used a smart aggregate (SA) to conduct an impact localization experiment on a concrete column. In the most studies, lead zirconite titanite (PZT) patches were usually employed as the sensors to receive the structural responses due to their performances of fast response, wide frequency band, and low cost. However, a drawback of these PZT patches are that the sensing direction mainly concentrates along the patch thickness, but the impact signals can come from random orientations, as shown in **Figure 1A**. Consequently, the loss of signals from other paths can lead to a decrease in the localization accuracy. Fortunately, with the development of sensor technology, Kong *et al.* redesigned a novel smart spherical aggregate (SSA) that replaced the traditional PZT patch with a spherical piezoceramic shell (SPS) which can function in omni-direction based on its radial vibration characteristic (Wang et al., 2016; Kong et al., 2017a; Kong et al., 2017b; Fan et al., 2021b), as shown in **Figure 1B**. The optimized SPS is able to sense the structural responses from random directions and provide the possibility of omni-directional detection. The functionality and performance of a single SPS have been investigated. However, to comprehensively understand a structural state, multiple sensors are usually required to be implemented on the host structure to capture the structural responses. The received signals of these collaborated sensors are used to quantify the structural damages and locate the damage/impact positions. The functional characteristic of multiple SPSs in SHM has not been investigated yet.

Over the past years, many efficient methods for localization of the impact source have been reported. Shrestha et al. (2017) developed an error outlier-based impact localization algorithm to study low-velocity impacts on a composite wing structure. De Simone et al. (2017) proposed a novel algorithm without the known material property to achieve impact source localization in aerospace composite structures. Among these existing researches, the time difference of arrival (TDOA) technique is one of the most popular and mature methods that have been applied in underwater, aircraft, highway, and tunnel for various AE localization (Chen et al., 2011; Hu et al., 2017; Hao et al., 2020; Wen et al., 2020). The key step of the TDOA technique is to precisely estimate the time-difference of the source signal to two receivers, which is highly affected by environmental noise, dispersion and attenuation of waves, and sensitivity of the sensors. The cross-correlation (CC) function, by measuring the similarity of two time series, is widely used for the calculation of TDOA (Benesty et al., 2004; Du et al., 2018). In addition, in 1976, Knapp and Carter (1976) proposed a generalized cross-correlation (GCC) function to optimize the traditional CC for accurate estimation of the TDOA. However, the applications of these methods are highly limited by experimental noise and signal frequency bandwidth.

To improve the accuracy of the estimation of TDOA for source localization, this article proposes an enhanced cross-correlation (ECC) algorithm enabled by a designed concrete implantable module (CIM). The CIM can be implanted into a concrete structure for SHM and also be pulled out for transducer updating. The design procedures of the CIM are introduced in detail. The principle of localization of the impact source and the proposed ECC algorithm for estimation of TDOA are theoretically interpreted. For precise estimation of a TDOA value, first, according to two received signals in an impact event, a cross-power spectrum and auto-power spectrum can be calculated, respectively, to enhance the signal-to-noise ratio (SNR) of the received signals. Subsequently, the two spectra correlate with a weight factor for estimation of the TDOA between the two signals. To validate the stability of the ECC algorithm under the noise condition, a numerical study was conducted. Finally, a series of impact tests on a concrete beam specimen were investigated to verify the accuracy of the proposed method for impact localization. The results show that using the

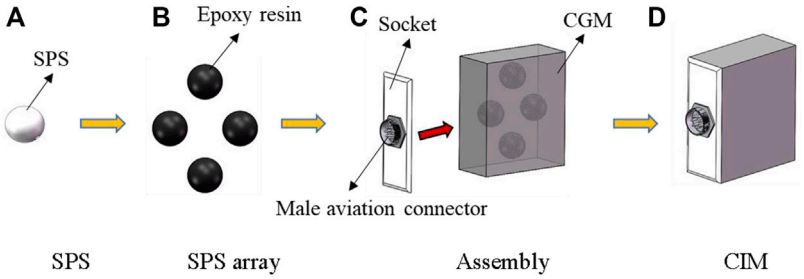

FIGURE 2 | Design procedures of the CIM. **(A)** SPS. **(B)** SPS array. **(C)** Assembly. **(D)** CIM.

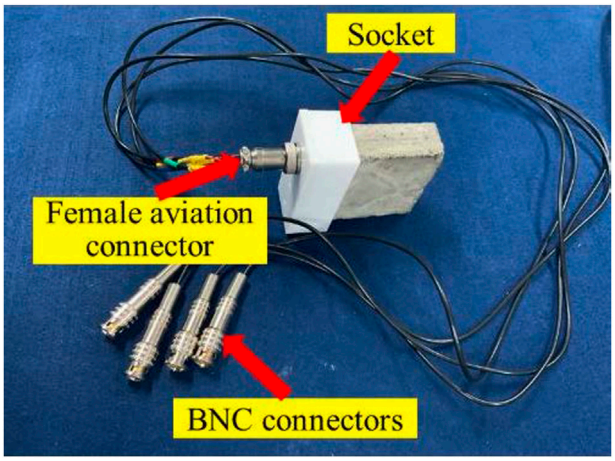

FIGURE 3 | Fabricated CIM model.

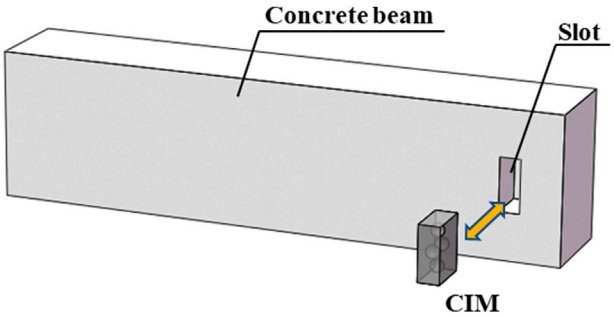

FIGURE 4 | Implanting the CIM into a concrete structure.

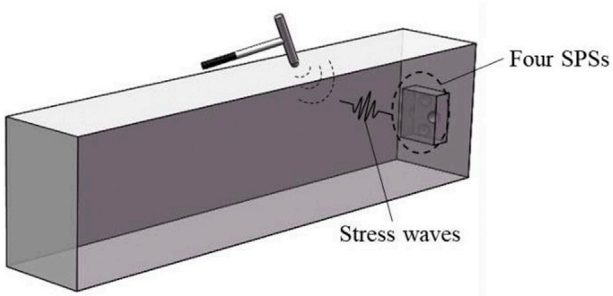

FIGURE 5 | Detection of the impact signals.

designed CIM to receive signals and the ECC algorithm to estimate the stress wave velocity and TDOA values, the impact locations can be predicted with an acceptable error. The proposed method exhibits a promising potential in SHM.

CIM AND LOCALIZATION PRINCIPLE

Introduction for the CIM

Motivated by the need to develop a novel practical device for SHM, the authors recently designed a CIM for SHM of concrete structures. In this article, the CIM is used to locate the impact source position based on the internal embedded sensing elements. **Figure 2** gives the detailed design procedures of the CIM. Spherical piezoceramic shell (SPS) with an excellent three-dimensional sensing ability was employed as the sensing element to receive the impact signals. Four waterproof resin-coated SPSs were arranged in a diamond array and encapsulated by a high-strength cement-based grouting material (CGM). A socket with a male aviation connector was attached to the module surface. The wires of SPSs were welded on the connector to communicate with the monitoring system. **Figure 3** presents a fabricated CIM with the dimensions of 25, 55, and 65 mm in three directions, respectively. To drive the CIM, a female aviation connector with four wires corresponding to the four SPSs was designed and inserted into the socket. The CIM can be implanted into a concrete structure with a reserved slot to monitor the structural dynamic responses, as shown in **Figure 4**.

Principle of the Impact Localization Based on the Diamond Array

When an impact event occurs at a random point on the concrete structure, the impact signals spread around in the form of stress waves, as shown in **Figure 5**. The implanted CIM can sense the structural dynamic responses and receive the impact signals

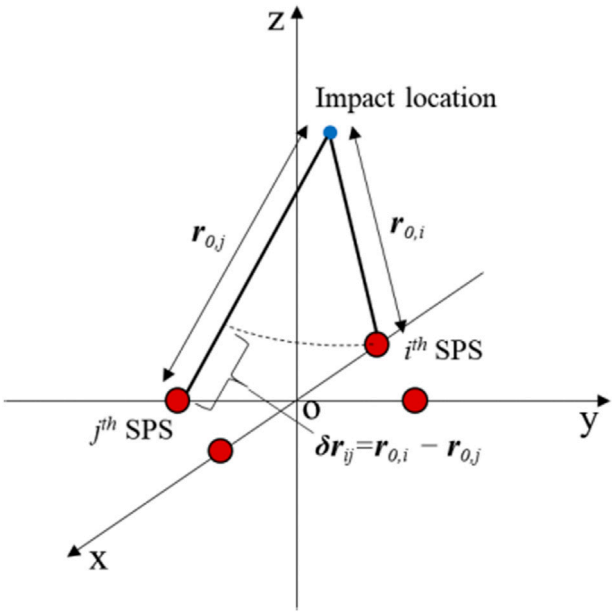

FIGURE 6 | Principle of the impact localization based on the diamond array.

relying on the SPS diamond array. The received signals can be used to determine the impact location based on the time-difference of each pair of SPSs, which is interpreted in detail as follows:

As shown in **Figure 6**, first, we assume that an impact event is located at r_0. For the ith (i = 1, 2, 3, and 4) SPS at r_i, its distance to the impact point can be denoted as $r_{0,i}$. The distance-difference of the impact location to the two SPSs can be represented as:

$$\left\|\mathbf{dr}_{ij}\right\| = \left\|\left(\mathbf{r}_0 - \mathbf{r}_i\right) - \left(\mathbf{r}_0 - \mathbf{r}_j\right)\right\| = \left\|\mathbf{r}_{0,\mathrm{i}} - \mathbf{r}_{0,\mathrm{j}}\right\| = \left(\boldsymbol{\tau}_{0,\mathrm{i}} - \boldsymbol{\tau}_{0,\mathrm{j}}\right)\mathbf{v}, \quad (1)$$

where $\tau_{0,i}$ and $\tau_{0,j}$ represent the time of flight (TOF) of the impact signals from the impact location to the ith SPS and jth SPS, respectively; v is the stress wave velocity in concrete structures. In general, v is estimated by the experiment. Let us define $d\tau_{ij}$ as the signal TDOA between the ith SPS and jth SPS:

$$d\tau_{ij} = \tau_{0,i} - \tau_{0,j}. \quad (2)$$

It should be noted that, when the impact signals are unknown, the TOF of $\tau_{0,i}$ and $\tau_{0,j}$ cannot be directly obtained. However, $d\tau_{ij}$ can be estimated without knowing impact signals with the help of ECC algorithm, which is explained in the next section. According to this, **Eq. 1** can be rewritten as:

$$\chi_{ij} = \left\|\mathbf{dr}_{ij}\right\| - d\hat{\tau}_{ij} \cdot \hat{\mathbf{v}}, \quad (3)$$

where χ_{ij} represents the residual caused by the estimation of $d\hat{\tau}_{ij}$ and $\hat{v}$. Ideally, when $d\hat{\tau}_{ij} = d\tau_{ij}$ and $\hat{v} = v$, the residual $\chi_{ij} = 0$.

By summing up the residuals between any two SPSs, the total impact localization residual η can be defined as:

$$\eta \triangleq \sum_{1 \le i < j \le N} \chi_{ij}, \quad (4)$$

where N is the number of SPSs. By searching the minimum value of η, the impact location r_0 can be evaluated.

ECC Algorithm for Estimation of TDOA

The traditional CC and GCC algorithms have been widely used for estimation of the TDOA between two receivers (Benesty et al., 2004; Meng et al., 2015; Du et al., 2018). However, the applications of these methods are highly limited by experimental noise and signal frequency bandwidth. To depress the noise and improve the accuracy of the estimated TDOA, this article proposes an ECC algorithm; the TDOA estimated by this algorithm will be used to localize the impact source in a concrete structure. The ECC algorithm can be explained as follows:

First, the signal received by the ith (i = 1, 2, 3, 4) SPS can be described as:

$$x_i(t) = s_0(t) \otimes h_{0,i}(t) + n_i(t), \quad (5)$$

where "⊗" represents the convolution operation, $s_0(t)$ is the impact source signal, $h_{0,i}(t)$ is the channel impulse response from the impact location to the ith SPS, and $n_i(t)$ means the noise from the environment. In addition, assuming only one impact source in the structure, $h_{0,i}(t)$ can be expressed as:

$$h_{0,i}(t) = \alpha_{0,i}\delta\left(t - \tau_{0,i}\right), \quad (6)$$

where $\alpha_{0,i}$ is an amplitude decay factor, $\delta(t)$ is the Dirac function, and $\tau_{0,i}$ represents the TOF from the impact location to the ith SPS. Substituting **Eq. 6** into **Eq. 5**, $x_i(t)$ can be written as:

$$x_i(t) = \alpha_{0,i}s_0\left(t - \tau_{0,i}\right) + n_i(t). \quad (7)$$

To estimate the TDOA between the ith SPS and jth SPS, their received signals $x_i(t)$ and $x_j(t)$ were used to calculate the cross-correlation and auto-correlation functions as two enhanced signals to improve SNR, respectively. The cross-correlation function $R_{x_ix_j}(\tau)$ can be represented as:

$$\begin{aligned} R_{x_ix_j}(\tau) &\triangleq \int_{-\infty}^{\infty} x_i^*(t)x_j(t+\tau)dt, \\ &= \int_{-\infty}^{\infty}\left[\alpha_{0,i}^*s_0^*\left(t-\tau_{0,i}\right) + n_i^*(t)\right]\left[\alpha_{0,j}s_0\left(t-\tau_{0,j}+\tau\right) + n_j(t)\right]dt, \\ &= \int_{-\infty}^{\infty}\left[\alpha_{0,i}^*\alpha_{0,j}s_0^*\left(t-\tau_{0,i}\right)s_0\left(t-\tau_{0,j}+\tau\right) + \alpha_{0,i}^*s_0^*\left(t-\tau_{0,i}\right)n_j(t)\right. \\ &\quad \left. + \alpha_{0,j}s_0\left(t-\tau_{0,j}+\tau\right)n_i^*(t) + n_i^*(t)n_j(t)\right]dt, \end{aligned} \quad (8)$$

where $(\cdot)^*$ denotes a complex conjugation. Assuming that the experimental noise is a white Gaussian noise and irrelevant to the impact signals, **Eq. 8** can be simplified as:

$$R_{x_ix_j}(\tau) = \alpha_{0,i}^*\alpha_{0,j}\int_{-\infty}^{\infty} s_0^*\left(t-\tau_{0,i}\right)s_0\left(t-\tau_{0,j}+\tau\right)dt. \quad (9)$$

Expressing the impact source signal as a frequency form, $R_{x_ix_j}(\tau)$ can be rewritten as:

$$\begin{aligned} R_{x_ix_j}(\tau) &= \alpha_{0,i}^*\alpha_{0,j}\int_{-\infty}^{\infty} S_0^*(f)S_0(f)e^{j2\pi f\left(\tau-\tau_{0,i}-\tau_{0,j}\right)}df, \\ &= \alpha_{0,i}^*\alpha_{0,j}\left\|S_0(f)\right\|^2\delta\left(\tau-\tau_{0,i}-\tau_{0,j}\right), \end{aligned} \quad (10)$$

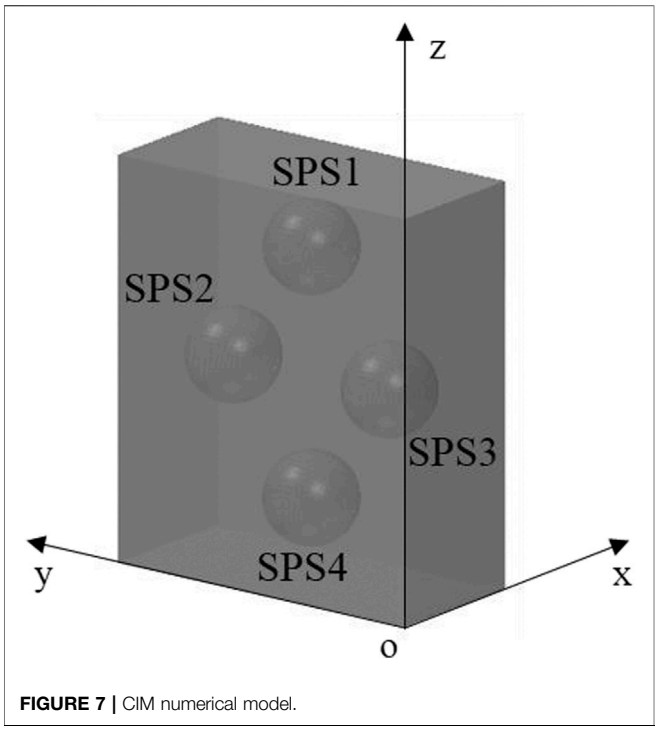

FIGURE 7 | CIM numerical model.

where $S_0(f)$ is the Fourier transform pair of $s_0(t)$. Notably, in **Eq. 10**, $R_{x_i x_j}(\tau)$ is still a time-domain expression. We can take the Fourier transform to $R_{x_i x_j}(\tau)$

$$\begin{aligned} R_{x_i x_j}(f) &= \mathcal{F}\left\{R_{x_i x_j}(\tau)\right\} \\ &= \alpha_{0,i}^{*}\alpha_{0,j}\left\|S_0(f)\right\|^2 \int_{-\infty}^{\infty} \delta\left(\tau - \tau_{0,i} - \tau_{0,j}\right) e^{-j2\pi f\tau} d\tau, \\ &= \alpha_{0,i}^{*}\alpha_{0,j}\left\|S_0(f)\right\|^2 e^{-j2\pi f\left(\tau_{0,i}+\tau_{0,j}\right)}. \end{aligned} \tag{11}$$

Actually, the $R_{x_i x_j}(f)$ is the cross-power spectrum of $x_i(t)$ and $x_j(t)$.

In the same way, the auto-power spectrum $R_{x_i x_i}(f)$ of the $x_i(t)$ can be represented as:

$$R_{x_i x_i}(f) = \left\|\alpha_{0,i}\right\|^2 \left\|S_0(f)\right\|^2 e^{-j4\pi f\tau_{0,i}}. \tag{12}$$

Subsequently, a cross-correlation function is established between the power spectra of $R_{x_i x_j}(f)$ and $R_{x_i x_i}(f)$ to obtain the final TDOA as follows:

$$RR_{x_i x_j}(\tau) \triangleq \int_{-\infty}^{\infty} \Psi(f) R_{x_i x_j}^{*}(f) R_{x_i x_i}(f) e^{j2\pi f\tau} df, \tag{13}$$

where $\Psi(f)$ is a weight factor that represents the phase transform (PATH). The $\Psi(f)$ can be defined as:

$$\Psi(f) \triangleq \frac{1}{\left\|R_{x_i x_j}^{*}(f) R_{x_i x_i}(f)\right\|}. \tag{14}$$

Substituting **Eq. 14** into **Eq. 13**, $RR_{x_i x_j}(\tau)$ can be described as:

$$RR_{x_i x_j}(\tau) = \int_{-\infty}^{\infty} \frac{R_{x_i x_j}^{*}(f) R_{x_i x_i}(f)}{\left\|R_{x_i x_j}^{*}(f) R_{x_i x_i}(f)\right\|} e^{j2\pi f\tau} df. \tag{15}$$

TABLE 1 | SPS and impact locations.

Subject	Location (mm)
SPS1	(12.5, 27.5, 52.5)
SPS2	(12.5, 42.5, 32.5)
SPS3	(12.5, 12.5, 32.5)
SPS4	(12.5, 27.5, 12.5)
Impact1	(0, 42.5, 12.5)
Impact2	(12.5, 0, 22.5)
Impact3	(12.5, 12.5, 65)

Notably,

$$\begin{aligned} \frac{R_{x_i x_j}^{*}(f) R_{x_i x_i}(f)}{\left\|R_{x_i x_j}^{*}(f) R_{x_i x_i}(f)\right\|} &= \frac{\alpha_{0,i}\alpha_{0,j}^{*}\left\|S(f)\right\|^2 \left\|\alpha_{0,i}\right\|^2 \left\|S(f)\right\|^2 e^{j2\pi f\left(\tau_{0,j}-\tau_{0,i}\right)}}{\left\|\alpha_{0,i}\alpha_{0,j}^{*}\left\|S(f)\right\|^2 \left\|\alpha_{0,i}\right\|^2 \left\|S(f)\right\|^2\right\|} \\ &= e^{j2\pi f\left(\tau_{0,j}-\tau_{0,i}\right)}. \end{aligned} \tag{16}$$

Therefore,

$$RR_{x_i x_j}(\tau) = \int_{-\infty}^{\infty} e^{j2\pi f\left(\tau+\tau_{0,j}-\tau_{0,i}\right)} df = \delta\left(\tau + \tau_{0,j} - \tau_{0,i}\right). \tag{17}$$

Substituting **Eq. 2** into **Eq. 17**, $RR_{x_i x_j}(\tau)$ can be described as:

$$RR_{x_i x_j}(\tau) = \delta\left(\tau - d\tau_{ij}\right). \tag{18}$$

The $d\hat{\tau}_{ij}$ can be estimated by searching the maximum value of $RR_{x_i x_j}(\tau)$as follows:

$$d\hat{\tau}_{ij} = \arg\max RR_{x_i x_j}(\tau). \tag{19}$$

STABILITY ANALYSIS OF THE ECC ALGORITHM

In localization of a sound source, it is greatly significant to precisely estimate the time difference of two signals, which is highly affected by the environmental noise, signal frequency bandwidth, and other adverse factors. To validate the stability of the proposed ECC algorithm in noise suppression, a numerical study was carried out. A CIM model was established by ABAQUS software (in **Figure 7**); three different impacts acted on the CIM surfaces. The special locations of the internal SPSs and the impacts are listed in **Table 1**. The impact behaviors were simulated by inputting a burst force on the CIM surfaces. The embedded SPSs could individually sense the structural responses and transform them into the potential signals to output. The inputting signal and outputting signals of each SPS were calculated along with their TOFs between the impact location and each SPS, respectively, based on the ECC algorithm. To investigate the stability of the algorithm, for each SPS, the received signals were manually added with white Gaussian noises with SNR of 10, 5, 0, -5, and -10 dB to simulate different levels of background noises. These noise-added signals successively calculated the TOFs; the percent errors of these noise-added TOFs relative to the

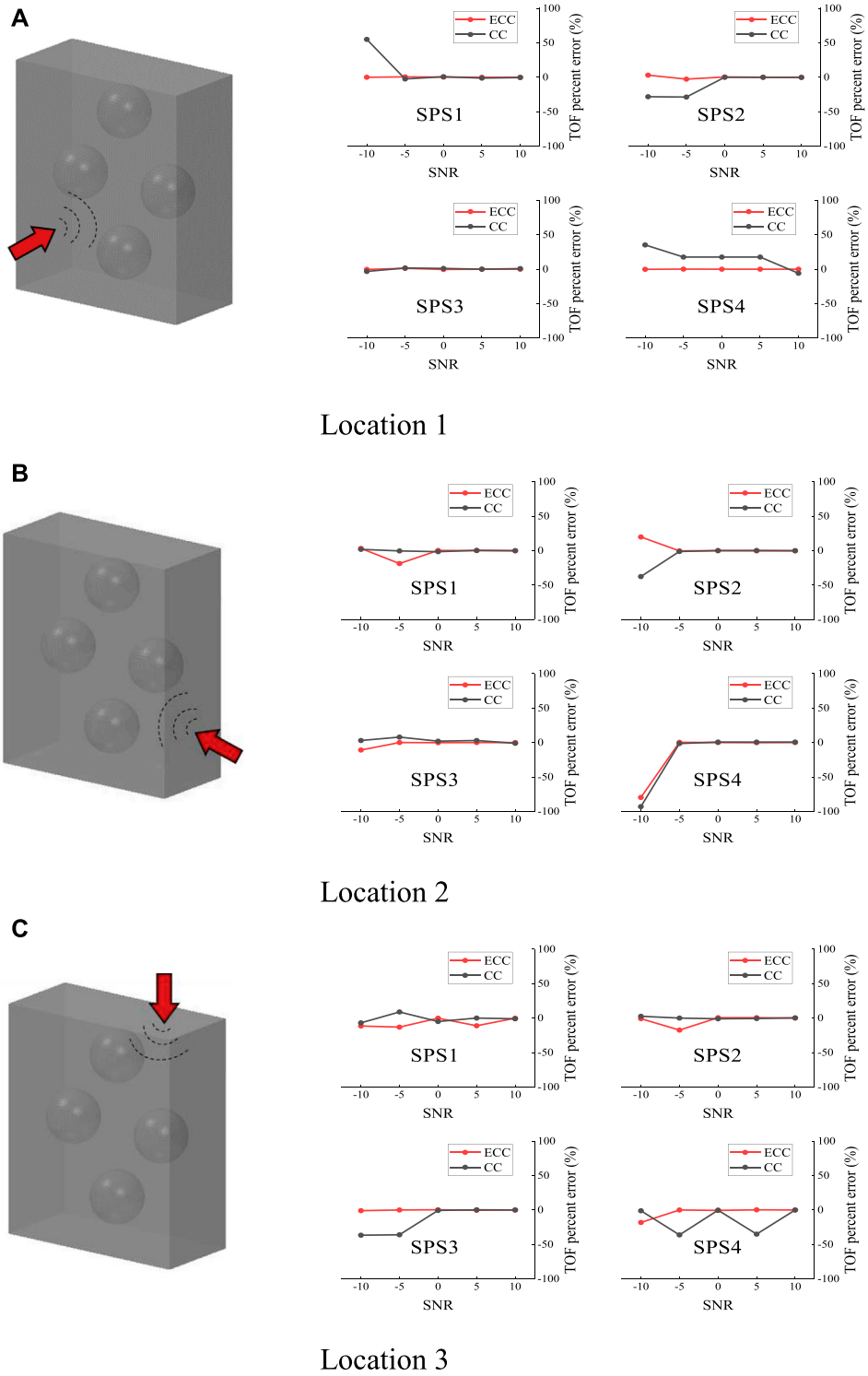

FIGURE 8 | TOF percent errors using ECC and CC algorithms. **(A)** Location 1. **(B)** Location 2. **(C)** Location 3.

corresponding original TOFs were selected as the index to describe the results. In addition, to contrastingly analyze the results, the traditional CC algorithm was used to calculate the TOFs and the percent errors following the aforementioned steps. The TOF errors using the ECC and CC algorithms are shown in **Figure 8**.

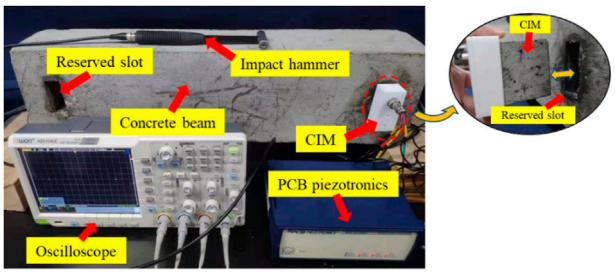

FIGURE 9 | Experimental setup.

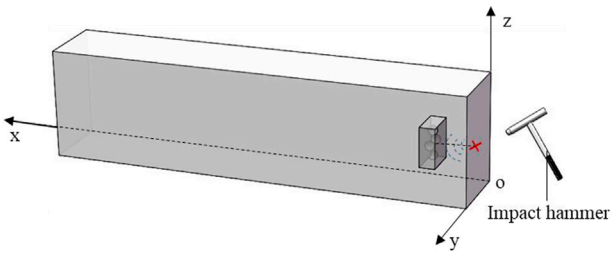

FIGURE 10 | Measurement method for the estimation of stress wave velocity.

It can be seen that, when the SNR is high, the TOF errors from ECC and CC algorithms are much close to 0. With the reduction of SNR, the TOF errors based on the CC algorithm perform obvious fluctuation. Conversely, the errors from the ECC algorithm remain with excellent stability. When the SNR reduces to −10 dB, the TOF errors from both the ECC and CC algorithms show sharp deviation. It can be concluded that, when the SNR > −10 dB, the ECC algorithm presents a stronger amticapability than the CC algorithm, which provides the possibility for employing this approach in real concrete structures.

EXPERIMENTAL STUDY

Experimental Setup

To verify the accuracy of the proposed method for localization of the impact sources, a series of impact tests were experimentally conducted on a concrete beam specimen. The specimen has a length, width, and height of 700, 120, and 180 mm, respectively. Two rectangular slots, of same size to the CIM, were reserved during the casting concrete process. In this study, the localization of single impact source was investigated and only the slot on the right side of the specimen was to install the CIM. To enhance the interface compatibility between the CIM and the beam specimen, proper ultrasonic coupling agent was used to fill the gap.

The experimental setup is shown in **Figure 9**. In addition to the concrete beam specimen, an oscilloscope as a multichannel data acquisition system was used to record the SPS signals; the oscilloscope was triggered by a voltage at the level of 2 mV; the sample frequency was set at 12.5 MHz. PCB piezotronics is a signal conditioner that can output the impact mechanical signals generated by the hammer. As can be seen in **Eqs 3**, **4**, the estimation of the stress wave velocity and the estimation of TDOA values of each pair of the SPSs are two key steps for the localization of the impact sources. The subsequent studies will concentrate on the two steps.

Estimation of the Stress Wave Velocity

It is of importance to precisely estimate the velocity of the stress waves propagating in the specimen for an accurate localization. However, the wave velocity is highly affected by the real material properties of Young's modulus and Poisson's ratio and density. It is not reasonable to estimate it only using some theoretical formulas. To precisely estimate the stress wave velocity, an experimental

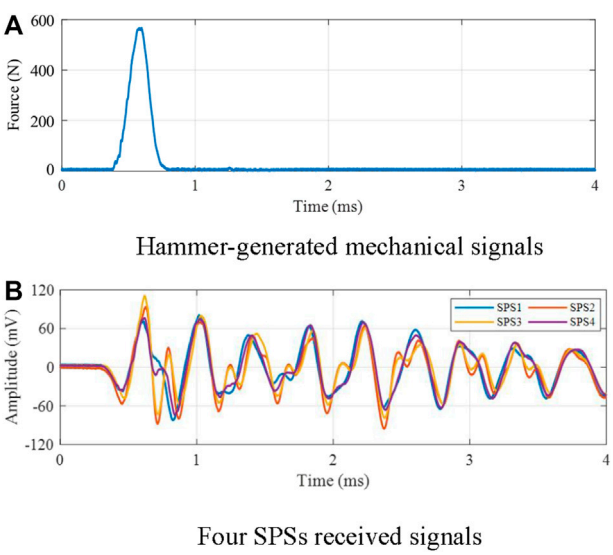

FIGURE 11 | Hammer-generated mechanical signals and SPS-received signals. **(A)** Hammer-generated mechanical signals. **(B)** Four SPS-received signals.

measurement was conducted. The measurement method can be described as follows: as shown in **Figure 10**, first, we can select a point to impact it, and meanwhile, the mechanical signals generated by the hammer. Then, the SPS-received signals can be extracted using the oscilloscope. Subsequently, by using the known impact source signals and its location, the TOFs between the impact point and each SPS can be calculated based on the ECC algorithm. Finally, according to the TOF values and their corresponding propagation distances, the stress wave velocity can be estimated. There, the projection of the CIM center on the side of the beam was selected as the impact point. To improve the accuracy, a total of five impacts were conducted for an average value. **Figure 11** shows the hammer-generated mechanical signals and the SPS-received signals in an impact measurement. **Table 2** lists the five test results of each SPS for the estimation of the stress wave velocity.

Impact Tests and Calculation of the TDOA

To verify the accuracy of the proposed method for localization of the impact sources, a total of eight impact tests, where the impact

TABLE 2 | Estimation of the stress wave velocity.

SPS	Location (mm)	Distance to impact point (mm)	TOF (ms)					Estimated average velocity (m/s)
			Test 1	Test 2	Test 3	Test 4	Test 5	
SPS1	(62.5, 92.5, 110)	65.62	0.0290	0.0270	0.0246	0.0241	0.0230	2552
SPS2	(62.5, 77.5, 90)	64.27	0.0290	0.0225	0.0226	0.0249	0.0272	
SPS3	(62.5, 107.5, 90)	64.27	0.0277	0.0275	0.0277	0.0326	0.0247	
SPS4	(62.5, 92.5, 70)	65.62	0.0230	0.0269	0.0237	0.0252	0.0219	

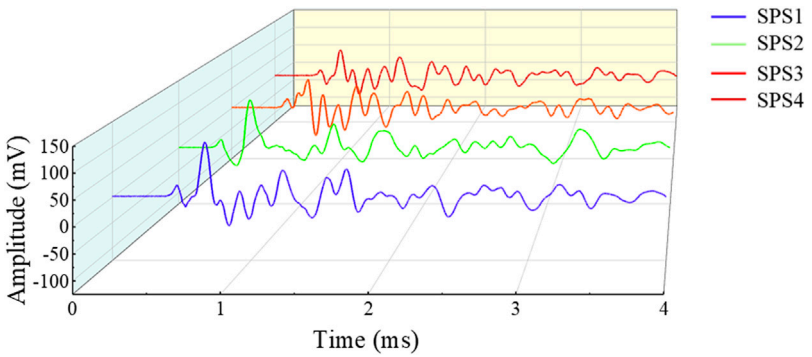

FIGURE 12 | Time-domain signals received by the CIM in test 1

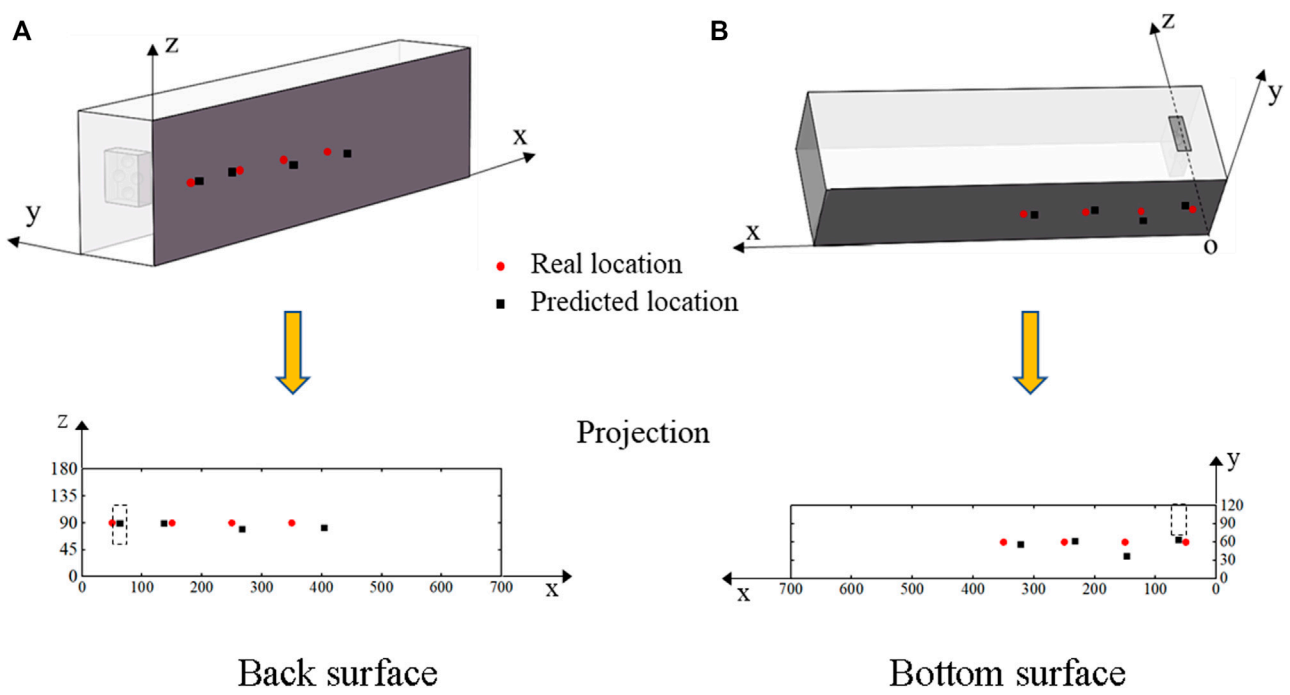

FIGURE 13 | Real and predicted impact locations and their projections on the beam surfaces. **(A)** Back surface. **(B)** Bottom surface.

locations were from the bottom and back surfaces of the concrete beam specimen corresponding to tests 1 to 8, were conducted. Notably, in these tests, the hammer-generated mechanical signals and impact locations were both unknown. The signals received by the four SPSs were extracted to calculate their TDOA values based on the ECC algorithm. **Figure 12** presents the CIM-received

TABLE 3 | Localization results.

Test		Real point (mm)	Estimated point (mm)	Distance error (mm)
Back	Test 1	(50, 0, 90)	(62.5, 0, 90.0)	12.5
	Test 2	(150, 0, 90)	(136.7, 0, 89.8)	13.3
	Test 3	(250, 0, 90)	(266.8, 0, 79.5)	19.8
	Test 4	(350, 0, 90)	(403.5, 0, 81.9)	54.1
Bottom	Test 5	(50, 60, 0)	(62.5, 64.1, 0)	13.2
	Test 6	(150, 60, 0)	(147.4, 36.8, 0)	23.3
	Test 7	(250, 60, 0)	(232.5, 61.9, 0)	17.6
	Test 8	(350, 60, 0)	(321.8, 56.6, 0)	28.4

signals in test 1. The TDOA values of $d\tau_{12}$, $d\tau_{13}$, and $d\tau_{14}$ were estimated as 0.00696, 0.00544, and 0.008 ms, respectively. For the other $d\tau_{ij}$, they can be converted with the three values. After estimating the stress wave velocity and TDOA values, the impact locations can be predicted by **Eq. 4**. Since **Eq. 4** is an overdetermined nonlinear set of equations, a least square method was used to search the optimal solution. In addition, the impact events can only occur on the beam surfaces, so the predicted locations were restrained on the surfaces.

Localization Results

According to the CIM-received signals under the eight tests, they were successively used to predict the impact locations based on the proposed method. The real and predicted impact locations and their projections on the corresponding beam surface are presented in **Figure 13**. **Table 3** lists the three-dimensional coordinates of each real and predicted impact locations. To quantify the accuracy of the predicted results, the distances between the real and corresponding predicted locations are calculated. It can be seen that the maximum distance error appearing in Test 4 is nearly 54.1 mm and the minimum distance error appearing in Test 1 is 12.5 mm. Relative to the large beam specimen sizes, the predicted locations from eight tests performed acceptable accuracy. It should be noted that, since the four SPSs arrange in a plane, as if a mirror, for each impact test, the predicted locations theoretically appear in pairs and symmetrically distribute on both sides of the mirror. However, due to the manufacturing defect on the CIM, the four SPSs are difficult to exactly arrange in the same plane; the mirror symmetrical locations do not exist.

Facing the predicted errors, several possible reasons are discussed. First, the SPSs own 7 mm radius that is neglected in the experiment by assuming as a point. The neglected radius is not small enough to the distance error. Second, the stress wave velocity is regarded as an isotropic constant in all paths. However, the multiphase composite concrete material can induce the stress wave velocity, which is anisotropic in the detected space; the estimated average velocity can be inaccurate in some paths. Third, when determining the SPSs' coordinates, the influence of the gap between the CIM and beam slot and the manufacturing defect on the CIM is not considered.

To further analyze the relationship between the impact positions and the localization accuracy, the x-coordinates of the impact positions and the corresponding distance errors are estimated as shown in **Figure 14**. From the line chart, with the impact positions away from the CIM, the distance errors almost rise monotonically. A possible reason is that the incremental travelling path of the stress waves in concrete could lead to a complex dispersion and mode-conversion, which obviously changes the stress wave velocity.

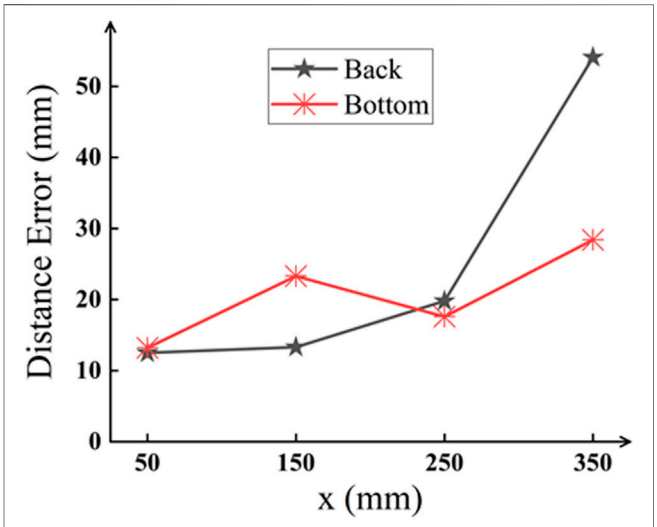

FIGURE 14 | Relationship between the impact locations and the distance errors.

DISCUSSION

The possible reasons of the predicted errors have been analyzed in the last section and can be summarized as the manufacturing defect, SPS size, stress wave velocity, and existing gaps between the CIM and beam slot. To overcome these drawbacks and improve the localization accuracy, more precise and deeper investigations are needed to be conducted.

Because the beam component is nearly a one-dimensional object, the arrangement of the SPSs is adopted as a diamond array in a plane whose normal line is along the length of the beam. For other different types of components, the shape of the CIM and the distribution and orientation of the internal SPSs can be optimized according to the detected goals. In addition, this technique requires a small slot reserved on the structure. The slot size

and location should minimize the negative effects on the structural load-bearing capacity.

The proposed method for localization of a single impact was validated using one CIM and a hammer generating an impact load. To localize several impact sources simultaneously, multiple CIMs with different orientations should be employed to collect impact-induced stress wave signals. Meanwhile, the current algorithm should be optimized to adapt for the identification of multiple impact loads using CIMs, which will be further investigated. In an impact event, except for prediction of the impact position, estimation of the impact energy is also significant to access the degree of structural damage and the residual structural load-bearing capacity. Since the attention coefficient of the stress waves propagating in the concrete medium can be measured, according to the SPS-received signals, the impact energy can be approximately estimated, which will be deeply investigated in future.

CONCLUSION

This article proposes an ECC algorithm for localization of the single impact source in concrete structures using a CIM that can be implanted into a concrete structure to sense the structural responses caused by an impact event. A CIM contains a SPS diamond array as the sensing element and an encapsulated layer to protect the fragile SPSs; its detailed design procedures were introduced. The numerical study demonstrates that when used for the estimation of the TOF values, the ECC algorithm has higher stability than the traditional CC algorithm under the interference of noises and provides the possibility for employing this method in concrete structures. In the experimental study, eight impact tests were conducted on a concrete beam specimen. By estimating the stress wave velocity and the TDOA values of each pair of SPSs based on the proposed ECC algorithm, the impact positions were predicted. The results validate the accuracy of the proposed method for localization of the impact sources. For adapting to different concrete components, the CIM shape and the SPSs' distribution and orientation can be optimized. In the future, improvement of the localization accuracy and estimation of the impact energy will both be investigated.

DATA AVAILABILITY STATEMENT

The raw data supporting the conclusion of this article will be made available by the authors, without undue reservation.

AUTHOR CONTRIBUTIONS

QC: data analysis, methodology, and writing; ZY: experiment and methodology; XL: experiment; XS: experiment; QK: funding acquisition and review.

FUNDING

The authors sincerely acknowledge the support from the National Natural Science Foundation of China (Grant Numbers: 51978507 and 52020105005).

REFERENCES

Aitcin, P. C. (2003). The Durability Characteristics of High Performance Concrete: a Review. *Cem. Concr. Compos.* 25 (4-5), 409–420. doi:10.1016/s0958-9465(02)00081-1

Asencio-Rhine, M. (2020). Available at: https://www.tampabay.com/news/2020/05/06/the-sunshine-skyway-bridge-plunged-into-tampa-bay-40-years-ago/.

Benesty, J., Chen, J., and Huang, Y. (2004). Time-delay Estimation via Linear Interpolation and Cross Correlation. *IEEE Trans. Speech Audio Process.* 12 (5), 509–519. doi:10.1109/tsa.2004.833008

Chen, H. B., Zhou, M., Gan, S. Y., Nie, X., Xu, B., and Mo, Y. L. (2021). Review of Wave Method-Based Non-destructive Testing for Steel-Concrete Composite Structures: Multiscale Simulation and Multi-Physics Coupling Analysis. *Constr. Build. Mater.* 302 123832. doi:10.1016/j.conbuildmat.2021.123832

Chen, L., Liu, Y. C., Kong, F. C., and He, N. (2011). "Acoustic Source Localization Based on Generalized Cross-Correlation Time-Delay Estimation," in *Ceis 2011*. Editors C. Ran and G. Yang (Amsterdam: Elsevier Science Bv). doi:10.1016/j.proeng.2011.08.915

De Fenza, A., Petrone, G., Pecora, R., and Barile, M. (2017). Post-impact Damage Detection on a Winglet Structure Realized in Composite Material. *Compos. Struct.* 169, 129–137. doi:10.1016/j.compstruct.2016.10.004

De Simone, M. E., Ciampa, F., Boccardi, S., and Meo, M. (2017). Impact Source Localisation in Aerospace Composite Structures. *Smart Mat. Struct.* 26 (12), 13. doi:10.1088/1361-665x/aa973e

Dong, L., Sun, D., Li, X., and Du, K. (2017). Theoretical and Experimental Studies of Localization Methodology for AE and Microseismic Sources without Pre-measured Wave Velocity in Mines. *IEEE Access* 5, 16818–16828. doi:10.1109/access.2017.2743115

Du, P., Zhang, S., Chen, C., Alphones, A., and Zhong, W.-D. (2018). Demonstration of a Low-Complexity Indoor Visible Light Positioning System Using an Enhanced TDOA Scheme. *Ieee Photonics J.* 10 (4), 831. doi:10.1109/jphot.2018.2841831

Ebrahimkhanlou, A., and Salamone, S. (2017). Acoustic Emission Source Localization in Thin Metallic Plates: A Single-Sensor Approach Based on Multimodal Edge Reflections. *Ultrasonics* 78, 134–145. doi:10.1016/j.ultras.2017.03.006

Ebrahimkhanlou, A., and Salamone, S. (2018). Single-Sensor Acoustic Emission Source Localization in Plate-like Structures Using Deep Learning. *Aerospace* 5 (2), 22. doi:10.3390/aerospace5020050

Fan, S., Zhao, S., Qi, B., and Kong, Q. (2018). Damage Evaluation of Concrete Column under Impact Load Using a Piezoelectric-Based EMI Technique. *Sensors (Basel)* 18 (5), 15. doi:10.3390/s18051591

Fan, X., Li, J., and Hao, H. (2021). Review of Piezoelectric Impedance Based Structural Health Monitoring: Physics-Based and Data-Driven Methods. *Adv. Struct. Eng.* 24 (16), 3609–3626. doi:10.1177/13694332211038444

Fan, S., Zhao, S., Kong, Q., and Song, G. (2021). An Embeddable Spherical Smart Aggregate for Monitoring Concrete Hydration in Very Early Age Based on Electromechanical Impedance Method. *J. Intelligent Material Syst. Struct.* 32 (5), 537–548. doi:10.1177/1045389x20963175

Feng, Q., Liang, Y. B., Tang, M., and Ou, J. P. (2020). Multi-parameter Monitoring for Steel Pipe Structures Using Monolithic Multicore Fibre Based on Spatial-Division-Multiplex Sensing. *Measurement* 164 108121. doi:10.1016/j.measurement.2020.108121

Hao, H., Hao, Y., Li, J., and Chen, W. (2016). Review of the Current Practices in Blast-Resistant Analysis and Design of Concrete Structures. *Adv. Struct. Eng.* 19 (8), 1193–1223. doi:10.1177/1369433216656430

Hao, K., Yu, K., Gong, Z., Du, X., Liu, Y., and Zhao, L. (2020). An Enhanced AUV-Aided TDoA Localization Algorithm for Underwater Acoustic Sensor

Networks. *Mob. Netw. Appl.* 25 (5), 1673–1682. doi:10.1007/s11036-020-01577-5

Hu, L., Liang, X., Zhang, J., Jing, X., and Zhang, J. (2017). Analysis on Optimal Formation Configuration of Three- Aircraft Cooperating Passive Location Using TDOA. *Fire Control Command Control* 42 (9), 49–54. doi:10.3969/j.issn.1002-0640.2017.09.011

Kao, C.-Y., and Loh, C.-H. (2013). Monitoring of Long-Term Static Deformation Data of Fei-Tsui Arch Dam Using Artificial Neural Network-Based Approaches. *Struct. Control Health Monit.* 20 (3), 282–303. doi:10.1002/stc.492

Knapp, C., and Carter, G. (1976). The Generalized Correlation Method for Estimation of Time Delay. *IEEE Trans. Acoust. Speech, Signal Process.* 24 (4), 320–327. doi:10.1109/tassp.1976.1162830

Ko, J. M., and Ni, Y. Q. (2005). Technology Developments in Structural Health Monitoring of Large-Scale Bridges. *Eng. Struct.* 27 (12), 1715–1725. doi:10.1016/j.engstruct.2005.02.021

Kocherla, A., Duddi, M., and Subramaniam, K. V. L. (2021). Smart Embedded PZT Sensor for *In-Situ* Elastic Property and Vibration Measurements in Concrete. *Measurement* 173 108629. doi:10.1016/j.measurement.2020.108629

Kong, Q. Z., Fan, S. L., Bai, X. L., Mo, Y. L., and Song, G. B. (2017). A Novel Embeddable Spherical Smart Aggregate for Structural Health Monitoring: Part I. Fabrication and Electrical Characterization. *Smart Mat. Struct.* 26 (9), 8. doi:10.1088/1361-665x/aa80bc

Kong, Q. Z., Fan, S. L., Mo, Y. L., and Song, G. B. (2017). A Novel Embeddable Spherical Smart Aggregate for Structural Health Monitoring: Part II. Numerical and Experimental Verifications. *Smart Mat. Struct.* 26 (9), 9. doi:10.1088/1361-665x/aa80ef

Meng, L., Li, X.-H., Zhang, W.-G., and Liu, D.-Z. (2015). "The Generalized Cross-Correlation Method for Time Delay Estimation of Infrasound Signal," in *Fifth International Conference on Instrumentation and Measurement, Computer, Communication and Control 2015*. Editor J. B. Li, 1320–1323.

Murthy, A., Palani, G., and Iyer, N. (2010). Impact Analysis of Concrete Structural Components. *Def. Sci. J.* 60 (3), 307–319. doi:10.14429/dsj.60.358

Perelli, A., De Marchi, L., Marzani, A., and Speciale, N. (2012). Acoustic Emission Localization in Plates with Dispersion and Reverberations Using Sparse PZT Sensors in Passive Mode. *Smart Mat. Struct.* 21 (2), 025010. doi:10.1088/0964-1726/21/2/025010

Rainieri, C., Fabbrocino, G., and Cosenza, E. (2011). Integrated Seismic Early Warning and Structural Health Monitoring of Critical Civil Infrastructures in Seismically Prone Areas. *Struct. Health Monit.* 10 (3), 291–308. doi:10.1177/1475921710373296

Schechinger, B., and Vogel, T. (2007). Acoustic Emission for Monitoring a Reinforced Concrete Beam Subject to Four-Point-Bending. *Constr. Build. Mater.* 21 (3), 483–490. doi:10.1016/j.conbuildmat.2006.04.003

Sedlak, P., Hirose, Y., and Enoki, M. (2013). Acoustic Emission Localization in Thin Multi-Layer Plates Using First-Arrival Determination. *Mech. Syst. Signal Process.* 36 (2), 636–649. doi:10.1016/j.ymssp.2012.11.008

Shrestha, P., Park, Y., and Kim, C.-G. (2017). Low Velocity Impact Localization on Composite Wing Structure Using Error Outlier Based Algorithm and FBG Sensors. *Compos. Part B Eng.* 116, 298–312. doi:10.1016/j.compositesb.2016.10.068

Tian, J. P., Zhang, J., Dong, F. F., and Du, G. F. (2019). Dynamic Response of Buried Pipeline Subject to Impact Loads Using Piezoceramic Transducers. *Int. J. Press. Vessels Pip.* 177, 11. doi:10.1016/j.ijpvp.2019.103984

Tsangouri, E., Karaiskos, G., Deraemaeker, A., Van Hemelrijck, D., and Aggelis, D. (2016). Assessment of Acoustic Emission Localization Accuracy on Damaged and Healed Concrete. *Constr. Build. Mater.* 129, 163–171. doi:10.1016/j.conbuildmat.2016.10.104

Wang, J. J., Kong, Q. Z., Shi, Z. F., and Song, G. B. (2016). Electromechanical Properties of Smart Aggregate: Theoretical Modeling and Experimental Validation. *Smart Mat. Struct.* 25 (9), 8. doi:10.1088/0964-1726/25/9/095008

Wang, Y., Chen, L., Wang, N., Gu, J., and Wang, Z. (2020). Three-dimensional Acoustic Emission Source Localisation in Concrete Based on Sparse Least-Squares Support Vector Regression. *Insight* 62 (8), 471–477. doi:10.1784/insi.2020.62.8.471

Wen, L., Han, J. K., Song, L. L., Zhang, Q., Li, K., Li, Z., et al. (2020). An Automated Real-Time Localization System in Highway and Tunnel Using UWB DL-TDoA Technology. *Wirel. Commun. Mob. Comput.* 2020, 15. doi:10.1155/2020/8877654

Xu, C., Gong, P., Xie, J., Shi, H., Chen, G., and Song, G. (2016). An Acoustic Emission Based Multi-Level Approach to Buried Gas Pipeline Leakage Localization. *J. Loss Prev. Process Industries* 44, 397–404. doi:10.1016/j.jlp.2016.10.014

Zhang, Y., Lu, W., and Chu, F. (2017). Planet Gear Fault Localization for Wind Turbine Gearbox Using Acoustic Emission Signals. *Renew. Energy* 109, 449–460. doi:10.1016/j.renene.2017.03.035

Zhu, J. X., Ho, S. C. M., Kong, Q. Z., Patil, D., Mo, Y. L., and Song, G. B. (2017). Estimation of Impact Location on Concrete Column. *Smart Mat. Struct.* 26 (5), 9. doi:10.1088/1361-665x/aa6768

Conflict of Interest: The authors declare that the research was conducted in the absence of any commercial or financial relationships that could be construed as a potential conflict of interest.

Publisher's Note: All claims expressed in this article are solely those of the authors and do not necessarily represent those of their affiliated organizations, or those of the publisher, the editors, and the reviewers. Any product that may be evaluated in this article, or claim that may be made by its manufacturer, is not guaranteed or endorsed by the publisher.

Copyright © 2022 Chen, Yang, Li, Sun and Kong. This is an open-access article distributed under the terms of the Creative Commons Attribution License (CC BY). The use, distribution or reproduction in other forums is permitted, provided the original author(s) and the copyright owner(s) are credited and that the original publication in this journal is cited, in accordance with accepted academic practice. No use, distribution or reproduction is permitted which does not comply with these terms.